Materials Research Proceedings 41 (2024) 70-79 https://doi.org/10.21741/9781644903131-8

Thermal multi-sensor instrumentation for the enhancement of a directed energy deposition process

DE PEINDRAY D'AMBELLE Lilou[1,a *], CHERRIER Olivier[1,b], MOUSSAOUI Kamel[1,c] and MABRU Catherine[1,d]

[1] Institut Clément Ader (ICA), UMR-CNRS 5312, 3 rue Caroline Aigle, 31400 Toulouse, France

[a]lilou.de-peindray-d-ambelle@isae-supaero.fr, [b]olivier.cherrier@isae-supaero.fr, [c]kamel.moussaoui@isae-supaero.fr, [d]catherine.mabru@isae-supaero.fr

Keywords: Additive Manufacturing, Powder Laser Metal Deposition, Instrumentation

Abstract. Directed energy deposition (DED) is an additive manufacturing process with growing industrial interests. Nonetheless, its industrialization will not be possible until it is fully mature. Such maturity lies in the upstream research to optimize and control it. In DED, process parameters, physical quantities and parts properties are interrelated which makes it a complex process. To have a better understanding of these relations, the experimental approach of instrumentation has been chosen. Multi-sensor method has been implemented for its more extensive possibilities in comparison to single-sensor methods. A bichromatic pyrometer was coupled to an IR camera to measure the temperature distributions in real time. Post-process characterizations of the aspects and geometries of the parts were related to the sensors' measurements and consequently, to the process parameters. Twelves sets of parameters were tested to conclude that the energy input impacts the size of the melting pool and the temperature distribution. High energies lead to defects such as edge defects and layer thickening but can mitigate surface roughness. Both the pyrometer and camera proved to have a relevance in this study for the enhancement of the DED process.

Introduction

Emerging metal additive manufacturing (MAM) processes such as Directed energy deposition (DED) are developed to be industrialized in sectors such as aeronautics and space [1,2]. This freeform direct deposition technique enables the reparation of components, the fabrication of functionally graded materials and the production of parts larger than with Laser Powder-Bed Fusion (LPBF). Moreover, this process meets with the new requirements of sustainable manufacturing. DED involves several parameters (key parameters are laser power P, scanning speed V and powder feed rate D_m) which are governing the physical quantities. These quantities affect in-process and post-process part properties. Among in-process properties is the bead geometry influenced by thermal phenomena such as the cooling rate and thermal gradients. Bead geometry features are linked to the melting pool where the heat input is located and where melting takes place. Post-process part properties have been studied quite broadly in literature, giving the microstructural, roughness, hardness, geometrical aspects of the component [3,4]. Common defects have been brought to the fore: lack of fusion porosities, cracks, anisotropy, substrate separation, part distortion and surface roughness. Once again, these defects are mostly related to thermal phenomena creating residual stresses and heterogeneities [5,6].

From these considerations, thermal phenomena seem to be one key to better understand DED. Process instrumentation, alongside process simulation, is a suitable candidate for the traceability of physical quantities during fabrication. Experimental approaches have been implemented to acquire more knowledge about the relation between process parameters, physical quantities, and part properties. Most studies focus on thermal aspects using a single sensor, generally infrared (IR) cameras and pyrometers [7–10]. The observations made with these sensors give an insight to the causes of geometrical and/or microstructural defects. The use of a single sensor to study the

process is though limited by parameters' interrelations and interdependence that are characteristic of MAM. Consequently, multi-sensor methods have been newly explored to combine the observations of several process signatures [11].

In this work, a thermal multi-sensor instrumentation was implemented in a DED machine. Both sensors are dedicated to measure temperature evolutions and distributions in real-time. In-process observations were correlated to the part's geometrical features. On the one hand, relevance of thermal multi-sensor approach was explored. On the other hand, the effect of thermal quantities and process inputs were linked to the properties of the part. Perspectives for further investigation of this method will be given.

Materials and methods

A 5-axis DED machine was used with argon as carrying and shielding gas. The power source is a Nd:YAG fiber laser with a maximal input power of 500 W. Building material was 316L stainless steel powder (Amperprint 0717 grade 1.4404, Höganäs) with particle size ranging from 45 to 90 µm. The powder composition is given in Table 1. 40 mm-long single-bead walls were constructed on 5 mm thick substrates. Each wall is programmed to reach a theoretical height of 15 mm. The deposition strategy (schemed Fig. 1) consisted of a two-way with a 3 s-dwell time between each layer. 12 walls were built according to a design of experiments varying P and V with a fixed value of D_m=6.5 g/min. In this study, P= {250,300,350,400} W and V= {600,900,1200} mm/min. Layer heights have been experimentally obtained with preliminary tests on single beads not described in this paper.

Table 1. Chemical composition of the 316L powder

Chemical composition [w%]	Cr	Ni	Mo	Mn	Si	C	P	S	O	N	Fe
Min	16.5	10.0	2.0	0.15	-	-	-	-	-	-	Balance
Max	18.5	14.0	3.0	2.0	1.0	0.03	0.045	0.015	0.05	0.03	

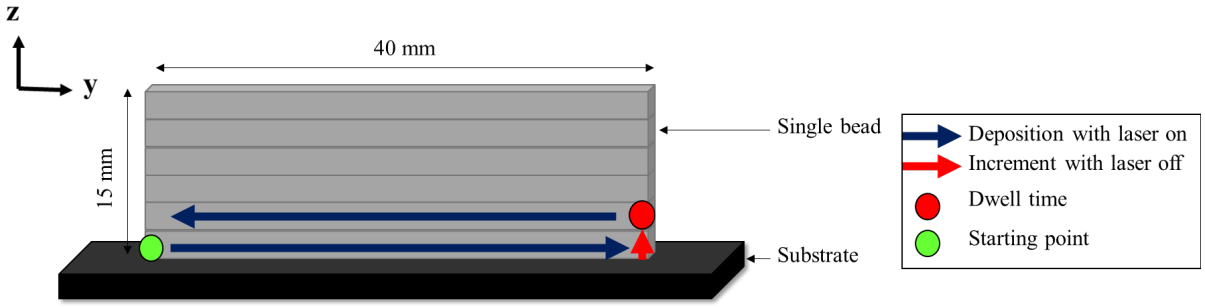

Figure 1. Deposition of the single-bead wall geometry

The instrumentation of the process consisted of an IR camera (PI08M, Optris) and a bichromatic pyrometer (CTRatio 2MH1, Optris). The camera is mounted on a support to observe the wall perpendicularly at 200 mm (distance between lens and laser axis). The resolution of the camera is 764x480 pixels for a recording framerate of 32 Hz. Its spectral range is 780-820 nm with a temperature range of 625-1900 °C. The bichromatic pyrometer was mounted on the deposition head and adjusted to measure perpendicularly to the wall also. The laser spot was aligned to the deposition axis 150 mm away from the wall. The pyrometer's spot is positioned to measure right underneath the layer that is being deposited. It has a temperature range of 550-3000 °C and a time resolution of 1 msec. The entire setup is shown Fig. 2.

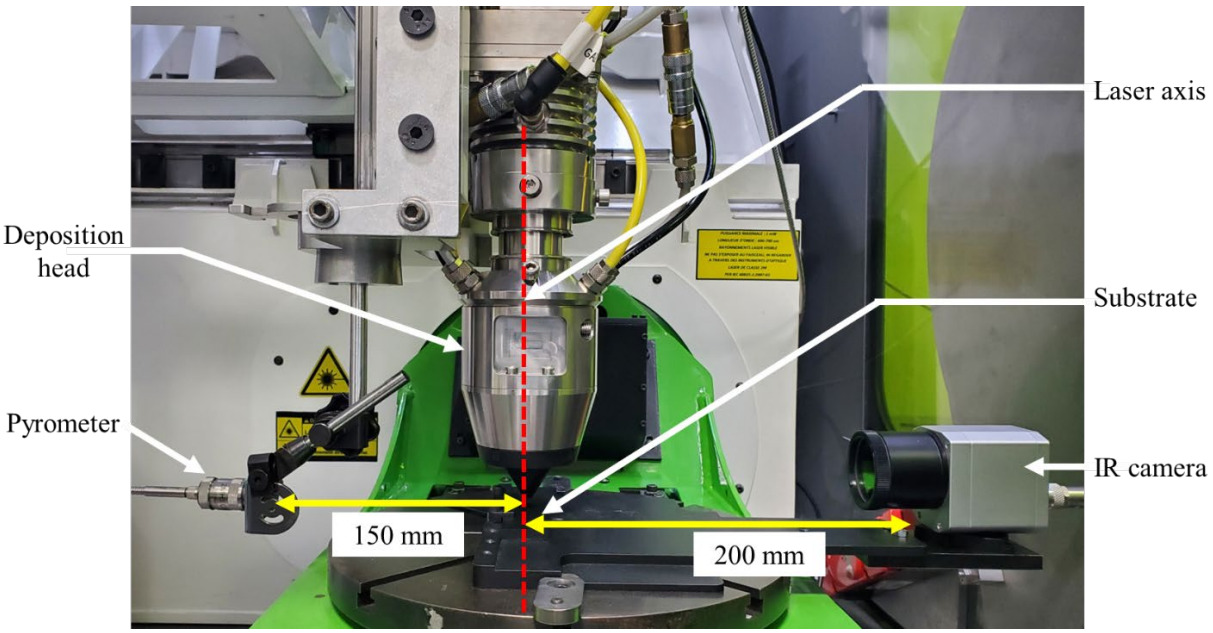

Figure 2. Experimental setup

The pixel size was determined with the ImageJ software thanks to the known distances in mm. It has been concluded that each pixel has a size of 0.25x0.25 mm^2. On IR images, the melting pool was identified as the area where the temperature exceeds the melting point of the material. In this study, the melting pool was set at 1400 °C.

Optical microscopy was conducted using a numerical microscope (VHX-970F, Keyence) to observe the general aspects of built walls. Mean final height was determined for each wall using a measuring column (LH-600D/DG, Mitutoyo) with 5 measure points along the top of the wall.

Results and discussion

Height measurements

Fig.3 compares the results of the mean height to the theoretical height of the walls.

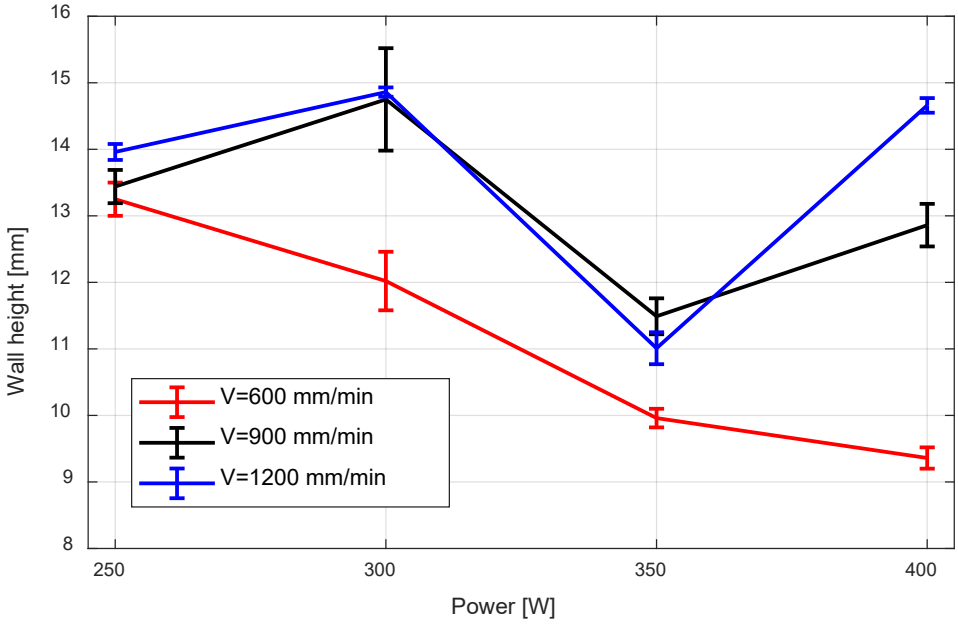

Figure 3. Final mean wall height as a function of process parameters P and V

Out of the 12 tests, only 3 of them, P300V900 and P400V1200 and P300V1200, reached approximately the desired final height. The other tests lead to small to important defocusing of the laser during construction. Fig. 3 shows that increasing the energy input (ratio between laser power and scanning speed) leads to final heights that are smaller than the theoretical height. This phenomenon is due to the use of constant laser power during construction. Indeed, along the wall, there will be more and more radial heat dissipation leading to an increase of the melt pool flow due the Marangoni effect [12]. Moreover, it is possible to observe that with small scanning speed V=600 mm/min, the final height of the walls is more affected than with the other speeds. Slow speed can lead to the widening of the melt pool and the flattening of the deposit because of higher dilution. This phenomenon has be shown in [13–15] and is more important when increasing P. Hence, the layers will become uneven, and the overall height will be smaller than planned. The results in Fig. 3 bring to the foreground the impact of key parameters on part's geometrical features. Nonetheless, an optimized set of parameters, such as P300V900 and P80V1200 in this study, could lead to components with final dimensions matching the model.

Optical microscopy

Examples of optical micrographs are shown Fig. 4. For this wall built with P=300 W and V=900 mm/min, the layers seem regular at the bottom of the part. The middle and top part of the wall have fewer regular layers and the latter form an interlacing. Along a single layer, the height varies. This effect is more visible on Fig. 5.

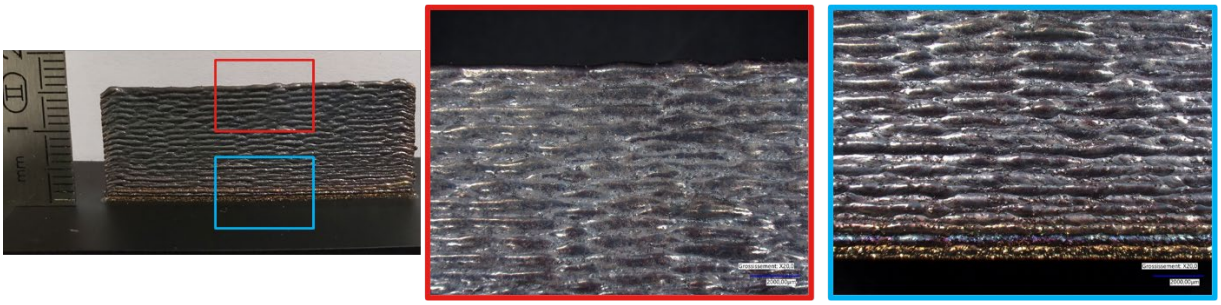

Figure 4. Example of a built wall (P300V900) and optical micrographs from the top middle part and the bottom middle part. Magnification x20

On Fig. 5, the interlacing effect is important for P300V900 and P400V900. The input parameters influence the form and aspect of the built layers. When the energy is lower, for instance at P400V900, the layers are more regular and straighter. These interlacing are due to the important heat input and are visible on every wall except for the ones built with P=250 W. The hypothesis is that when the energy is too high, the deposited layer might significantly melt the previous one and leads to the thickening of the current layer while flattening the previous one. This effect is not visible on the first layers because there is no heat accumulation at the beginning due to the heat conduction of the substrate. In addition, the walls built with lower energy input seem to be more rectangular than the higher energy ones which are curved and wavier. The edge effect on high energy walls is because at the start and stop points, the bead has less time to cool down. Consequently, the heat builds up and both ends of the wall collapse [16].

On the first micrograph (P250V900), there is an effect every other layer where one layer is thicker than the following. The regularity of this phenomenon might be related to the two-way deposition strategy of this study. Moreover, in each of these 3 cases, fused-on and unmolten particles are visible to the surface of the walls. With low energy input, particles are ejected from the melting pool and fuse to the surface of the deposit. It is not clear for now why the roughness changes every other layer, even if it still might be explained by the phenomena caused by the two-way deposition.

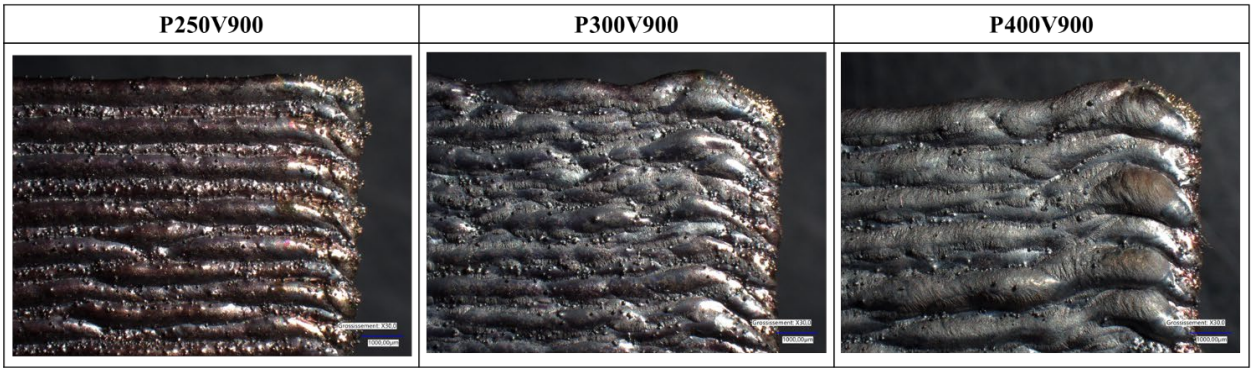

Figure 5. Optical micrographs of top right corner of walls for P250V900, P300V900 and P400V900. Magnification x30 with partial ring lighting

Thermal sensors measurements

Fig. 6 shows the images taken with the IR camera. The obtained temperatures are no absolute temperatures but relative ones because of the chosen constant value of the emissivity. The raw images without treatment are given Fig.6-a) and c). Fig. 6-b) and d) depict the melting pool enclosed by the blue line. For comparison, images from the 10th layer with P300V900 and P400V900 are shown. Because of higher power input, the heated zone in Fig. 6-d) is larger and contains higher temperatures than in Fig. 6-b). The melting pool has been enclosed and was zoomed out on Fig. 7. An estimation of the height and the width of this melting pool areas was done thanks to the knowledge of the pixel size. This measurement shows that higher power might lead to wider melting pool. The size of the melting pool is a data that can be related to the layer dimensions and will help to understand the aspects observed previously. This treatment of IR images and the robustness of this sensing approach will be confronted to literature, where the IR camera is usually positioned coaxially [16–18].

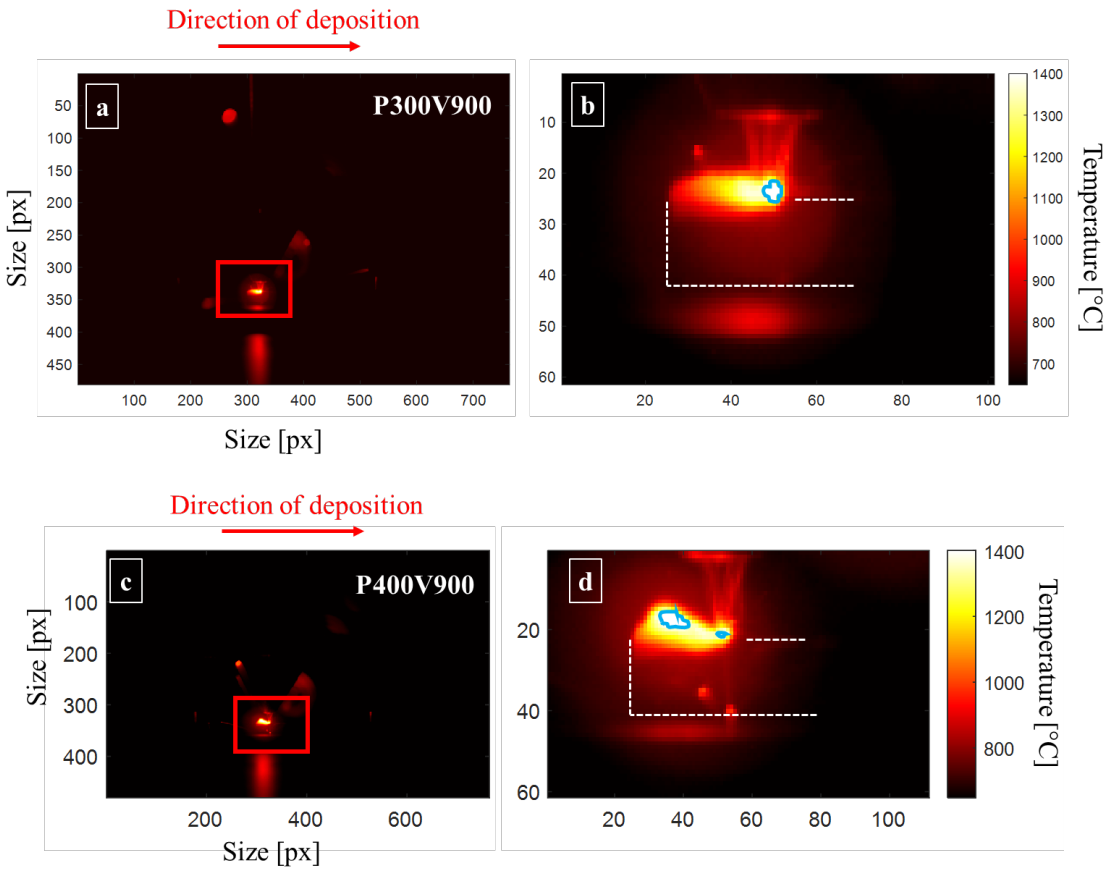

Figure 6. a)-c) Images obtained with the IR camera for P300V900 and P400V900 respectively. b)-d) Magnification of the previous images. The blue lines enclose the melting pools. The white dotted lines represent the edges of the walls.

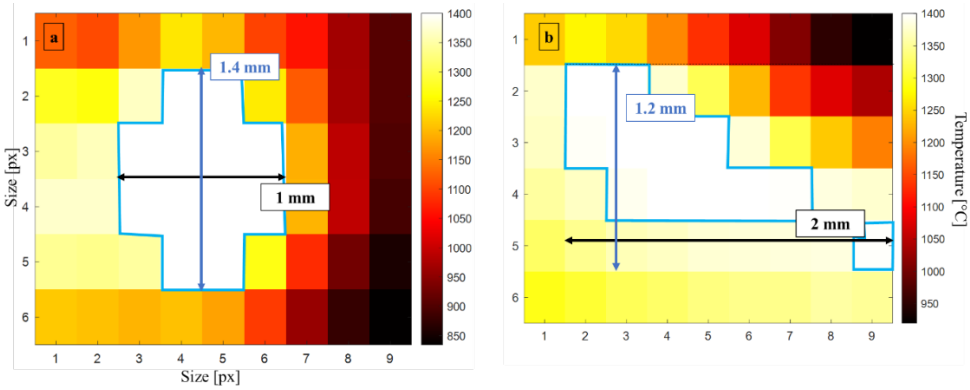

Figure 7. Estimation of melt pool height and width at the start of the 10th layer for a) P300V900 and b) P400V900.

Fig. 8 gives an example of the pyrometer's measurements during construction. For an energy input of 17 J, Fig. 8-a) represents the temperature evolution over time for the entire process while Fig. 8-b) focuses on the 5th and the 6th layers. The dwell time of 3 s can be noticed. At the beginning of construction, the pyrometer is just underneath the deposition and it takes a certain time for it (according to layer height) to start to measure. In addition, not all of the pyrometer's data was exploitable for the 12 tests because of defocusing. When the distance between the nozzle and deposit increases, the pyrometer's measure spot goes upward, the signal starts to saturate and eventually, there is no more signal.

The temperature-time diagram depicts the successive increases and decreases of temperature with some variations during deposition. These variations can be explained by the changes of the melt pool area along the layer making variations of the pyrometer's measurements. This phenomenon is consistent with the work of [19,20]. As shown in Fig. 8-b), the temperature of the 6th layer is higher and reaches a maximum of 1750 °C while the 5th layer reaches a maximum of 1650 °C. Furthermore, there is an increase of the global temperature during the process due to heat accumulation [21,22]. The peaks observed at both ends of the layer are related to the melting pool area that is warmer and wider at these points [16].

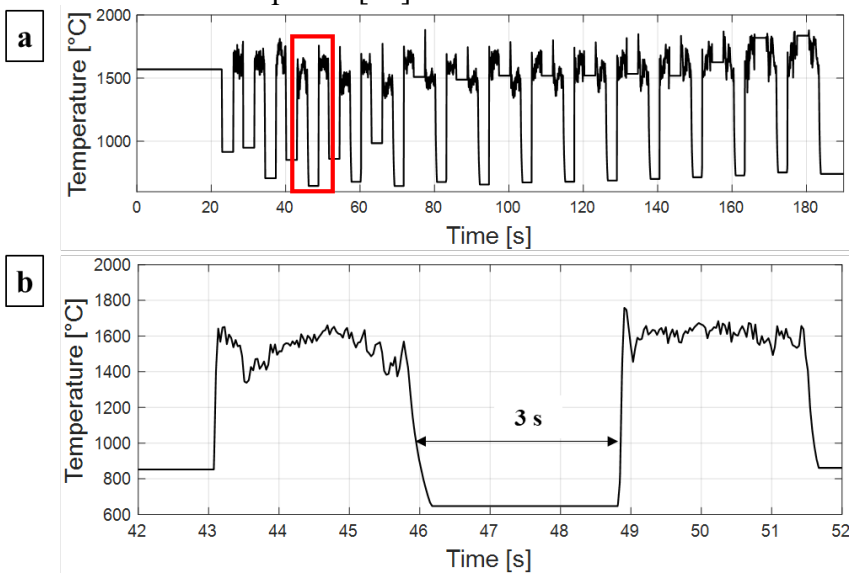

Figure 8. Pyrometer temperature-time diagrams during deposition with E= 17 J. a) Entire construction. b) Layer 5 and layer 6

Fig. 9 compares the temperature-time diagram of the pyrometer and the IR camera for the 5th and 6th layers. The diagram for the camera (in red) corresponds to the evolution of the maximum temperature over time. Both signals are similar and have the same order of magnitude. However, the pyrometer seems to measure more variations, and this might be caused by the fact that the pyrometer is attached to the deposition head and is probably submitted to more variations. This effect might also be due to the resolution of both sensors. One should also note that there is no noticeable work comparing pyrometry and IR thermography directly on the same build in literature to see if one sensor completes the other.

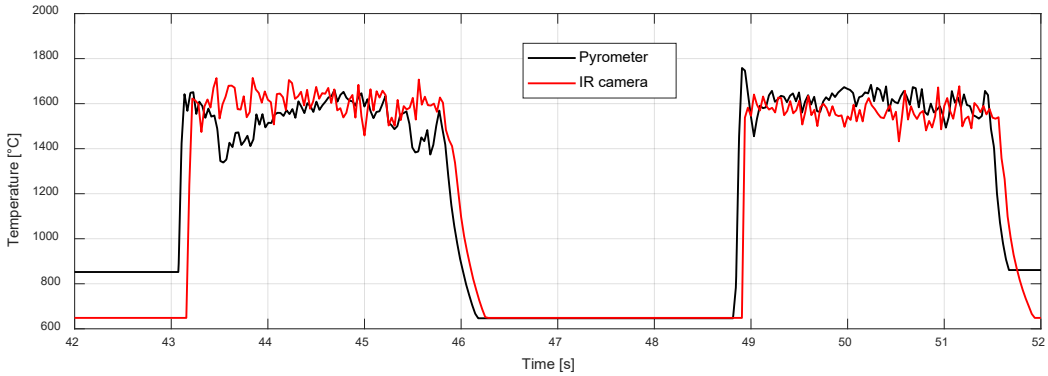

Figure 9. Temperature-time diagrams of 5th and 6th layers for E=17 J. Comparison between pyrometer and IR camera

Conclusions and future work

This work presents a thermal multi-sensor approach for a Directed energy deposition process. A series of twelve 316L single-bead walls varying the laser power and scanning speed was realized. Real-time measurements of the temperature with a fixed IR camera and an embedded pyrometer have been done. The aim of this study was to validate the relevance of the method, the sensors, and their combination. Each sensor gave exploitable results that were completed by post-process analyzes of geometrical features of the wall. With the design of experiments and the observations done, it is possible to relate some of the process parameters to the thermal distribution and eventually to the aspect of the wall:

- The increase of energy input has an influence on the size of the heated zone and the melting pool area which directly impacts the layer geometry. A high heat input leads to irregular, wavy and thick layers leading afterwards to a diminution of the overall height of the wall.
- Surface roughness of the wall is diminished by high energy input. It appeared that deposition strategy also has an important role in the parts final properties.
- The defocusing due to high energy input hindered a part of the measurements but the rest was exploitable. The signals depicted the influence of process parameters over heat accumulation and temperatures. Edge effects also could be related to the temperature peaks at both ends of the layer on the pyrometer's signal.
- The IR camera's images can be used to extract temperature data as well as the geometrical features of the heated zone and the melting area. This data corroborates the aspects of the wall and the measurements done with the pyrometer.
- The fixed position of the camera prevents it from getting some of the small variations observable with the pyrometer. It supports the use of both sensor for a more complete understanding of thermal phenomena. This approach will help to enhance the properties of DEDed parts.

Future work will be dedicated to several aspects:

- The development of an algorithm to have the evolution of the melting pool size
- The completion of the design of experiments with statistical study
- Further characterizations of the constructed wall thanks to cross-sectional views

References

[1] P. Gradl, D.C. Tinker, A. Park, O.R. Mireles, M. Garcia, R. Wilkerson, C. Mckinney, Robust Metal Additive Manufacturing Process Selection and Development for Aerospace Components, J. of Materi Eng and Perform 31 (2022) 6013–6044. https://doi.org/10.1007/s11665-022-06850-0

[2] B. Blakey-Milner, P. Gradl, G. Snedden, M. Brooks, J. Pitot, E. Lopez, M. Leary, F. Berto, A. du Plessis, Metal additive manufacturing in aerospace: A review, Materials & Design 209 (2021) 110008. https://doi.org/10.1016/j.matdes.2021.110008

[3] D. Herzog, V. Seyda, E. Wycisk, C. Emmelmann, Additive manufacturing of metals, Acta Materialia 117 (2016) 371–392. https://doi.org/10.1016/j.actamat.2016.07.019

[4] L. Zhu, P. Xue, Q. Lan, G. Meng, Y. Ren, Z. Yang, P. Xu, Z. Liu, Recent research and development status of laser cladding: A review, Optics & Laser Technology 138 (2021) 106915. https://doi.org/10.1016/j.optlastec.2021.106915

[5] S. Guo, C. Zamiela, L. Bian, Knowledge-transfer-enabled porosity prediction for new part geometry in laser metal deposition, Journal of Manufacturing Processes 103 (2023) 64–77. https://doi.org/10.1016/j.jmapro.2023.08.002

[6] M. Liu, A. Kumar, S. Bukkapatnam, M. Kuttolamadom, A Review of the Anomalies in Directed Energy Deposition (DED) Processes & Potential Solutions - Part Quality & Defects, Procedia Manufacturing 53 (2021) 507–518. https://doi.org/10.1016/j.promfg.2021.06.093

[7] M. Mazzarisi, A. Angelastro, M. Latte, T. Colucci, F. Palano, S.L. Campanelli, Thermal monitoring of laser metal deposition strategies using infrared thermography, Journal of Manufacturing Processes 85 (2023) 594–611. https://doi.org/10.1016/j.jmapro.2022.11.067

[8] A.J. Myers, G. Quirarte, J.L. Beuth, J.A. Malen, Two-color thermal imaging of the melt pool in powder-blown laser-directed energy deposition, Additive Manufacturing (2023) 103855. https://doi.org/10.1016/j.addma.2023.103855

[9] S.J. Altenburg, A. Straße, A. Gumenyuk, C. Maierhofer, In-situ monitoring of a laser metal deposition (LMD) process: comparison of MWIR, SWIR and high-speed NIR thermography, Quantitative InfraRed Thermography Journal 19 (2022) 97–114. https://doi.org/10.1080/17686733.2020.1829889

[10] C. Hagenlocher, P. O'Toole, W. Xu, M. Brandt, M. Easton, A. Molotnikov, The Effect of Heat Accumulation on the Local Grain Structure in Laser-Directed Energy Deposition of Aluminium, Metals 12 (2022) 1601. https://doi.org/10.3390/met12101601

[11] A. Chabot, M. Rauch, J.-Y. Hascoët, Towards a multi-sensor monitoring methodology for AM metallic processes, Welding in the World 63 (2019) 759–769. https://doi.org/10.1007/s40194-019-00705-4

[12] N. Ali, L. Tomesani, A. Ascari, A. Fortunato, Fabrication of Thin Walls with and without Close Loop Control as a Function of Scan Strategy Via Direct Energy Deposition, Lasers Manuf. Mater. Process. 9 (2022) 81–101. https://doi.org/10.1007/s40516-022-00164-8

[13] B.T. Gibson, Y.K. Bandari, B.S. Richardson, A.C. Roschli, B.K. Post, M.C. Borish, A. Thornton, W.C. Henry, M. Lamsey, L.J. Love, Melt Pool Monitoring for Control and Data Analytics in Large-Scale Metal Additive Manufacturing, in: University of Texas at Austin, 2019. https://doi.org/10.26153/tsw/17371

[14] M.F. Schneider, Laser Cladding with Powder: Effect of Some Machining Parameters on Clad Properties, 1998.

[15] B. Carcel, J. Sampedro, I. Perez, E. Fernandez, J.A. Ramos, Improved laser metal deposition (LMD) of nickel base superalloys by pyrometry process control, in: XVIII International Symposium on Gas Flow, Chemical Lasers, and High-Power Lasers, SPIE, 2010: pp. 643–651. https://doi.org/10.1117/12.878749

[16] D. Hu, R. Kovacevic, Sensing, modeling and control for laser-based additive manufacturing, International Journal of Machine Tools and Manufacture 43 (2003) 51–60. https://doi.org/10.1016/S0890-6955(02)00163-3

[17] M. Akbari, R. Kovacevic, Closed loop control of melt pool width in robotized laser powder–directed energy deposition process, Int J Adv Manuf Technol 104 (2019) 2887–2898. https://doi.org/10.1007/s00170-019-04195-y

[18] Y. Ding, J. Warton, R. Kovacevic, Development of sensing and control system for robotized laser-based direct metal addition system, Additive Manufacturing 10 (2016) 24–35. https://doi.org/10.1016/j.addma.2016.01.002

[19] A. Zapata, C. Bernauer, M. Hell, M.F. Zaeh, Studies on the direction-independent temperature measurement of a coaxial laser metal deposition process with wire, (n.d.).

[20] I. Smurov, M. Doubenskaia, A. Zaitsev, Comprehensive analysis of laser cladding by means of optical diagnostics and numerical simulation, Surface and Coatings Technology 220 (2013) 112–121. https://doi.org/10.1016/j.surfcoat.2012.10.053

[21] B. Wu, D. Ding, Z. Pan, D. Cuiuri, H. Li, J. Han, Z. Fei, Effects of heat accumulation on the arc characteristics and metal transfer behavior in Wire Arc Additive Manufacturing of Ti6Al4V, Journal of Materials Processing Technology 250 (2017) 304–312. https://doi.org/10.1016/j.jmatprotec.2017.07.037

[22] D. Yang, G. Wang, G. Zhang, Thermal analysis for single-pass multi-layer GMAW based additive manufacturing using infrared thermography, Journal of Materials Processing Technology 244 (2017) 215–224. https://doi.org/10.1016/j.jmatprotec.2017.01.024